The short-time dynamics of molecular reorientation in liquids. II. The microscopic mechanism of rotational friction

Joonkyung Jang, and Richard M. Stratt

Citation: The Journal of Chemical Physics **112**, 7538 (2000);
View online: https://doi.org/10.1063/1.481351
View Table of Contents: http://aip.scitation.org/toc/jcp/112/17
Published by the American Institute of Physics

The short-time dynamics of molecular reorientation in liquids. II. The microscopic mechanism of rotational friction

Joonkyung Jang and Richard M. Stratt
Department of Chemistry, Brown University, Providence, Rhode Island 02912

(Received 29 November 1999; accepted 7 February 2000)

At short times, the dynamics of the rotational relaxation of linear molecules dissolved in liquids is governed by the instantaneous rotational friction, a quantity one can specify in complete molecular detail for each liquid configuration. Having the ability to construct such a friction is not only useful for the insight it provides into rotational dynamics, it means that it is possible to think about the superficially very different processes of rotational relaxation, vibrational population relaxation and solvation in a common language. In particular, the ability to understand the friction in molecular terms allows us to compare the actual solvent molecules participating and the actual solvent motions involved in all of these relaxation processes. In this paper we carry out a detailed study of the rotational friction felt by a homonuclear diatomic molecule dissolved in an atomic fluid, contrasting the results for a variety of solute sizes and thermodynamic states. We find remarkable levels of similarity among all three kinds of relaxation. While there are some detailed differences in the geometry of the relevant solvent motions, all three processes seem to be controlled by a small number of nearby solvents. Possibly as a result, the influence spectra (the spectral densities) of all three are virtually identical. The invariance of these findings, and indeed of the mechanistic details, to solute size and thermodynamic conditions suggests that there is a real universality to solution dynamics that comes into play when sharply varying forces are involved. [S0021-9606(00)50317-1]

I. INTRODUCTION

The phrase ''rotational friction'' seems suggestive of a rather traditional view of rotational dynamics in liquids: that the rotation of small molecules in solution is largely a matter of rotational diffusion.[1] Up until relatively recently the experimental evidence was taken to be completely consistent with this presumption; there did seem to be some sort of rotational drag exerted by a solvent caused by its viscosity,[2] or perhaps by its bulk dielectric response,[3] which acted virtually instantaneously to convert the free rotation characteristic of the gas phase into the diffusive motion found in liquids. There were complications as to which particular boundary conditions were best suited to modeling the process with bulk hydrodynamics,[4] and there have been more recent studies pointing out the need to incorporate such features as realistic solute charge distributions[5] and different diffusion constants around different solute axes,[6] but the prospects for learning something about the microscopics of the *solvent* dynamics by looking at rotational friction always seemed antithetical to a continuum picture—which seemed more than ample for the experiments at hand.

A number of experiments have begun to appear, however, emphasizing the real need for a more molecular perspective on rotational relaxation. Zewail and co-workers,[7] in particular, have found that they could study the onset of diffusive motion by tracing the evolution of rotational dynamics starting with the gas phase and increasing the density, a process which all but calls out for an interpretation in terms of the changes in the motions of individual solvent neighbors. Similarly telling, Horng, Gardecki, and Maroncelli[8] have demonstrated, working from the liquid side, that continuum models cannot explain rotational dynamics in polar solvents by appealing to dielectric friction. Alcohols especially are poorly accounted for by such theories.

We can get some feeling for at least some of the issues involved in arriving at a microscopic theory by thinking about a set of rudimentary model problems: those posed by the reorientational dynamics of homonuclear diatomics of varying shapes (Fig. 1) dissolved in simple atomic liquids. Solving the classical dynamics of such systems is, of course, a routine matter for molecular dynamics simulations[9] and we portray in Fig. 2 the resulting dynamics for solutes ranging from nearly spherical to quite oblong. The angular velocity autocorrelation functions obtained,

$$C_{\omega\omega}(t)=\langle \vec{\omega}(t)\cdot\vec{\omega}(0)\rangle/\langle \vec{\omega}(0)\cdot\vec{\omega}(0)\rangle, \tag{1.1}$$

with $\vec{\omega}(t)$ the angular velocity of the solute, make it clear that this dynamics can span quite a range, even without the complications of Coulombic forces. The slow, picosecond decay with which the correlation is lost for the most spherical solutes indicates a nearly free rotation, whereas the 200 fs oscillation seen with the longest bond lengths implies a predominantly librational character to the motion—and the liquid time scales, correspondingly, run the gamut from diffusive to inertial. Presumably any sucessful theory for this problem must be robust enough, and microscopic enough, to encompass this diversity in its entirety.[9,10]

The theoretical approach we suggested in the companion paper to this one (paper I)[11] is to continue to focus on the origins of the rotational friction, but to do so fully molecu-

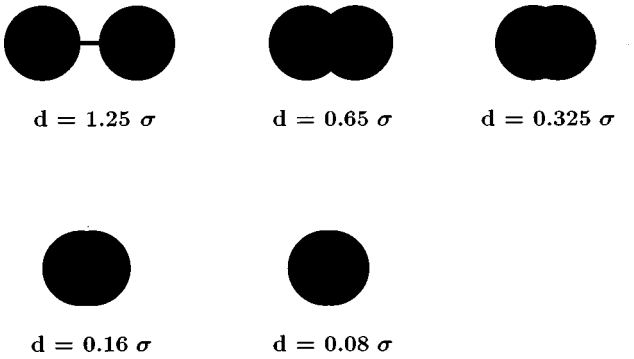

FIG. 1. The shapes and sizes of the diatomic solute molecules studied in this paper. The diatomics have a variety of bond lengths, d, but each atom on each diatomic is drawn as a sphere with diameter of σ, consistent with the choice of a single Lennard-Jones diameter σ for all the atoms involved in the model.

larly. To this end we showed that by considering separately the dynamics launched from each individual liquid configuration, one could derive what we called an instantaneous generalized Langevin equation,[12] one in which we could give a precise prescription for understanding how the necessary friction could be constructed from genuinely molecular ingredients. The friction so obtained was accurate only at short times, but rotational friction in liquids often does, in fact, have a rather short time scale, even when the overall relaxation is slow.[8,10,13,14] Our instantaneous friction therefore turned out to be in reasonably good agreement with the true friction obtained by molecular dynamics over most of the interesting frequency range.[11]

The key to our development was that we could represent the instantaneous dynamics of the liquid in terms of the solvent's instantaneous normal modes (INMs).[15,16] As in the linear INM theories of vibrational relaxation and solvation, the central quantity was what we referred to as an influence spectrum[17–19]

$$\rho(\omega)=\left\langle \sum_{\alpha} c_{\alpha}^{2}\delta(\omega-\omega_{\alpha})\right\rangle, \tag{1.2}$$

the spectrum of the INM frequencies ω_{α} for each liquid mode α, weighted by the coupling coefficients c_{α}, which embody the efficiency with which each mode affects the solute dynamics. With rotational relaxation, for example, the central issue is the ability of the modes to alter the torque felt by the solute.

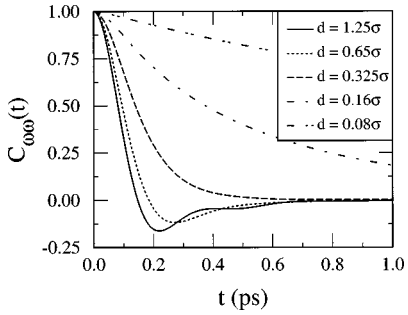

FIG. 2. The exact, normalized, angular-velocity autocorrelation functions for homonuclear diatomic solutes of different bond lengths d dissolved in dense supercritical argon ($\rho\sigma^3=1.05$, $k_BT/\epsilon=2.5$). The curves were calculated from the molecular dynamics simulations described in Sec. III.

The importance to us of this spectral representation is twofold: For one, we expect the rotational friction itself to be related quite directly to the rotational influence spectrum.[11] Since we have completely molecular interpretations of the modes and thus of the coupling coefficients, we should be able to discern the molecular mechanisms of rotational relaxation just by asking which sets of solvent motions end up contributing the most to the influence spectrum. Equally intriguing though, is the fact that a variety of very different solute relaxation processes can all be described by these influence spectra. We can therefore look for whatever commonalities there might be between solvation, vibrational relaxation, and rotational relaxation, asking whether the limited dynamical possibilities imposed by a common solvent are ever going to be enough to overcome the rather different symmetries and couplings of these distinct processes.[17,19] In this paper we will attempt to pursue both of these objectives.

The remainder of this paper is organized as follows: In Sec. II we summarize the route we took in paper I to obtain the rotational friction in terms of a rotational influence spectrum and we point out how one can extract the contributions of various physically relevant subsets of the solvent (and solute) motions from these influence spectra. We turn next to the numerics. The set of particular model systems we study has already been protrayed in Figs. 1 and 2, but we provide some more detail in Sec. III, along with the specifics for all of our calculations. Our results for the rotational friction spectrum (and, for comparison, for some examples of vibrational relaxation and solvation) are then presented in Sec. IV. We conclude in Sec. V with a discussion of some possible connections with other perspectives on rotational friction.

II. THEORETICAL BACKGROUND

A. Instantaneous rotational friction

We begin by briefly reviewing the instantaneous rotational generalized Langevin equation (GLE) formalism developed in paper I.[11] Consider, as we did there, a rigid homonuclear diatomic molecule dissolved in an atomic solvent and denote the orientation of the diatomic in the laboratory frame by the angles θ and ϕ, taking the remaining ''bath'' variables, $\mathbf{R}=(\vec{r}_0(t),\ldots,\vec{r}_N(t))$, to include both the center-of-mass position of the solute, $\vec{r}_0$, and the solvent atom positions, $\vec{r}_j$ $(j\geqslant 1)$. The Hamiltonian for this infinitely dilute solution can thus be written as

$$H=\frac{I}{2}(\dot{\phi}^2\sin^2\theta+\dot{\theta}^2)+\frac{1}{2}\sum_{j=0}^{N} m_j\dot{\vec{r}}_j^{\,2}+V(\phi,\theta,\mathbf{R}), \tag{2.1}$$

with I the moment of inertia of the diatomic and m_j the masses of the diatomic and the solvent atoms, $j=0$ and $j\geqslant 1$, respectively. The crucial step in deriving an instantaneous GLE from Eq. (2.1) is to expand the total potential, $V(\phi,\theta,\mathbf{R})$, in powers of the displacements from the initial configuration $(\phi_0,\theta_0,\mathbf{R}_0)$. If we truncate the expansion of

the bath part of the potential at second order in the displacements $(\mathbf{R}-\mathbf{R}_0)$, we are immediately led to introduce the bath instantaneous normal modes q_α,

$$q_\alpha = \sum_{j\mu} (m_j)^{1/2} U_{j\mu,\alpha}(r_{j\mu} - r_{j\mu,0}), \tag{2.2}$$

where μ labels the x, y, and z directions. Since the dynamics of such modes is straightforward,[20] subsequent expansion of the remainder of the potential and re-expression in terms of INMs allows us to write an explicit equation of motion for the angular velocity of the solute, one in which all of the bath effects are subsumed into an effective torque and a frictional response, both fully defined in molecular terms.

The instantaneous rotational friction that results is a reflection of what we have called the rotational friction spectrum of the bath, $\rho_{\rm fric}(\omega)$, defined as

$$\rho_{\rm fric}(\omega) = \left\langle \sum_\alpha (c_\alpha)^2 \delta(\omega - \omega_\alpha) \right\rangle, \tag{2.3}$$

where the average is over bath configurations and the coupling coefficients c_α indicate the extent to which the αth instantaneous normal mode, q_α, causes a torque on the solute

$$c_\alpha = -\frac{\partial N}{\partial q_\alpha}, \tag{2.4}$$

with N being the torque along the axis perpendicular to the bond axis of the diatom. In terms of this fundamental spectral response, the average time domain, $\eta^{\rm INM}(t)$, and frequency domain, $\tilde{\eta}^{\rm INM}(\omega)$, versions of the friction are simply

$$\eta^{\rm INM}(t) = \int d\omega\, \rho_{\rm fric}(\omega) \frac{\cos \omega t - 1}{\omega^2}, \tag{2.5}$$

$$\tilde{\eta}^{\rm INM}(\omega) = \int_0^\infty dt \cos \omega t\, \eta^{\rm INM}(t) = \frac{\pi}{2} \frac{\rho_{\rm fric}(\omega)}{\omega^2}. \tag{2.6}$$

The instantaneous GLE itself describes the reorientational dynamics of the solute for each liquid configuration, but a virtually quantitative reformulation allows us to see how the equation predicts the dynamics on the average. The angular-velocity autocorrelation function, $C_{\omega\omega}(t)$, generated from our averaged GLE, for example, evolves as

$$\dot{C}_{\omega\omega}(t) = -\int_0^t d\tau [\overline{\Omega}^2 + (1/I)\, \eta^{\rm INM}(t-\tau)] C_{\omega\omega}(\tau), \tag{2.7}$$

where the rms-*instantaneous-librational frequency*, $\overline{\Omega}$, is defined as

$$\overline{\Omega}^2 = \left\langle \frac{1}{I} \frac{\partial^2 V}{\partial \theta^2} \right\rangle. \tag{2.8}$$

Note that were the solvent held fixed at its initial configuration, the friction in Eq. (2.7) would vanish, and $C_{\omega\omega}(t)$ would behave as if the solute were a harmonic oscillator with frequency, $\overline{\Omega}$. The rms-librational frequency is thus a measure of the caging abilities of a hypothetically static solvent. Parenthetically, one might observe that it is the whole memory kernel in Eq. (2.7), $I\overline{\Omega}^2 + \eta^{\rm INM}(t)$, which plays the role of the exact friction, $\eta(t)$, in the more conventional formulations of the rotational GLE. The INM friction, by contrast, is defined to be initially zero, meaning that we should really think of it as the change in the friction between time t and time 0. Consistent with this idea, we see that we need to interpret $I\overline{\Omega}^2$ as $\eta(0)$, the time-zero value of the exact friction kernel. In fact, this identification is not only sensible, it is actually a rigorous result for the true friction.[21]

B. Influence spectra and their projections

The ability to cast the study of rotational dynamics into a form dependent on an influence spectrum means that there are going to be strong parallels to our studies of other solute-centered relaxation phenomena, such as vibrational relaxation[12,19,22] and solvation.[18] The basic (linearized) INM perspective is that one inevitably need to understand a spectral response of the form

$$\rho_A(\omega) = \left\langle \sum_\alpha \left(\frac{\partial A}{\partial q_\alpha} \right)^2 \delta(\omega - \omega_\alpha) \right\rangle, \tag{2.9}$$

for some ''spectroscopic probe function'' A in order to understand how a given solute degree of freedom relaxes.[17–19] The spectroscopic probe function for the rotational friction spectrum is the *torque* along the axis perpendicular to the bond direction unit vector, $\hat{e}$,

$$A = \frac{d}{2} [\hat{e} \times (\vec{F}_b - \vec{F}_a)]_\perp, \tag{2.10}$$

where $\vec{F}_b$ and $\vec{F}_a$ are the solvent forces on the two atoms of the diatomic, and $\perp$ denotes the component perpendicular to the bond axis. The vibrational friction spectrum results when A is identified as the *force* along the bond axis,

$$A = \tfrac{1}{2} \hat{e} \cdot (\vec{F}_b - \vec{F}_a). \tag{2.11}$$

Except for a factor of the bond length, d, the rotational and the vibrational friction spectra thus explore different projections of the same force on the solute. Solvation, superficially a rather distinct case, probes the *potential energy difference* between the ground and excited states of the solute. But, if we model solvation as an electronic excitation of a single atom and assume pair potentials, then the solvation spectrum becomes perfectly analogous, with

$$A = \sum_{j=1}^N v(r_{0j}), \tag{2.12}$$

where $v(r_{0j})$ is the change in the solute–solvent pair potentials between the two electronic states.[17–19]

Any influence spectrum written in the form of Eq. (2.9) automatically resolves the relaxation process into a distinct response for each frequency. More than that, however, the contributions of each coefficient, c_α can be broken into separate pieces from each solvent atom and each direction in space

$$c_\alpha = \sum_{j\mu} U_{j\mu,\alpha} c_{j\mu}, \quad c_{j\mu} = (m_j)^{-1/2} \frac{\partial A}{\partial r_{j\mu}}. \tag{2.13}$$

We should therefore be able to identify the mechanisms by which a relaxation occurs just by projecting these c_α onto particular directions relative to the solute or onto special sets of solvent atoms interacting with the solute. Indeed, this basic approach has been elaborated before,[18,19] but since these projections serve as our principal machinery for investigating the microscopics behind solvent friction, it is worth pausing to discuss how they work in our particular context here. This discussion will also allow us to introduce a slight improvement into how our projection techniques handle solute translation.

Regardless of the specific variety of solute relaxation, the coupling coefficients will always contain a contribution from the center-of-mass translation of the solute ($j=0$); this translation is, after all, one of the bath variables. In particular, for a solute with a relatively low molecular weight, the center-of-mass motion of the diatomic will be significantly coupled to rotational friction (about 25% of the total friction spectrum in our present study, where the solute is twice the mass of the solvent). However, this coupling can actually be expressed as a linear combination of the solvent atom contributions. Let us denote the coupling constant of the jth atom by the vector, $\vec{c}_j=(c_{jx},c_{jy},c_{jz})$. Momentum conservation (or equivalently, translational invariance) tells us that[23]

$$\vec{c}_0=-\sum_{j=1}^{N}\sqrt{\frac{m_j}{M}}\vec{c}_j, \tag{2.14}$$

with the solute mass $M\equiv m_0$, allowing us to write each c_α formally in terms of purely solvent-atom contributions

$$c_\alpha=\sum_{\substack{j=1\\ \mu}}^{N}\left(U_{j\mu,\alpha}-\sqrt{\frac{m_j}{M}}U_{0\mu,\alpha}\right)c_{j\mu}. \tag{2.15}$$

Using Eq. (2.15) is equivalent to using Eq. (2.13), but it will be helpful in our subsequent projections in that it will let us think physically about the solvent's effective contributions to relaxation.

The projection of influence spectra into two mutually orthogonal directions easily follows the development of Eq. (2.15). Suppose we want to project the spectra onto the directions specified by unit vectors, $\hat{b}$ and $\hat{b}^\perp(\hat{b}\cdot\hat{b}^\perp=0)$. Resolving the $\vec{c}_j$ into the $\hat{b}$ and $\hat{b}^\perp$ directions

$$\vec{c}_j=(\hat{b}\cdot\vec{c}_j)\hat{b}+[\vec{c}_j-(\hat{b}\cdot\vec{c}_j)\hat{b}], \tag{2.16}$$

lets us divide the mode coupling strength, c_α, into

$$c_\alpha=c_\alpha^b+c_\alpha^{\perp b}, \tag{2.17}$$

where the individual mode couplings projected into $\hat{b}$ and $\hat{b}^\perp$ directions are defined as

$$c_\alpha^b=\sum_\beta P_{\alpha\beta}^b c_\beta,\quad c_\alpha^{\perp b}=\sum_\beta P_{\alpha\beta}^{\perp b}c_\beta, \tag{2.18}$$

respectively, with the projectors, $\mathbf{P}^b$ and $\mathbf{P}^{\perp b}$ given as[24]

$$P_{\alpha\beta}^b=\sum_{\substack{j=1\\ \mu,\nu}}^{N}\left(U_{j\mu,\alpha}-\sqrt{\frac{m_j}{M}}U_{0\mu,\alpha}\right)b_\mu b_\nu U_{j\nu,\beta},$$

$$P_{\alpha\beta}^{\perp b}=\delta_{\alpha\beta}-P_{\alpha\beta}^b. \tag{2.19}$$

As a direct result of Eq. (2.17), given any arbitrary vector $\hat{b}$, an influence spectrum can always be written as a sum of parallel, perpendicular, and cross components

$$\rho_A(\omega)=\rho_A^b(\omega)+\rho_A^{\perp b}(\omega)+\rho_A^{\text{cross}}(\omega), \tag{2.20}$$

$$\rho_A^b(\omega)=\left\langle\sum_\alpha (c_\alpha^b)^2\delta(\omega-\omega_\alpha)\right\rangle, \tag{2.21}$$

$$\rho_A^{\perp b}(\omega)=\left\langle\sum_\alpha (c_\alpha^{\perp b})^2\delta(\omega-\omega_\alpha)\right\rangle, \tag{2.22}$$

$$\rho_A^{\text{cross}}(\omega)=\left\langle\sum_\alpha 2(c_\alpha^b)(c_\alpha^{\perp b})\delta(\omega-\omega_\alpha)\right\rangle. \tag{2.23}$$

One can, for example, take $\hat{b}$ to be the bond direction vector, $\hat{e}$, to project influence spectrum into directions *parallel* and *perpendicular* to the bond axis of the diatom. Similarly, the *longitudinal-transverse* projection is obtained by identifying $\hat{b}$ as the unit direction vector, $\hat{r}_{j0}$, from the center of mass of the diatom to the jth solvent atom.[22] In either case one can discern the fraction of the entire response associated with each projection by partitioning the total coupling strength, $C=\langle\Sigma_\alpha(c_\alpha)^2\rangle$, in much the same way as

$$C=C^b+C^{\perp b}+C^{\text{cross}}, \tag{2.24}$$

where the various C's on the right-hand side give the areas under the corresponding projected spectra.[18,19]

One is not limited, of course, to such abstract geometrical projections. We can also select out particular atoms instead of summing Eq. (2.15) over all the solvent atoms.[17,19] For each configuration, the solvent atoms nearest to the solute can be chosen to give the *nearest atom* projection, or we can obtain the *maximal atom* projection by picking out a single atom most strongly coupled with the solute for each mode.[25] For comparison we may also want to single out the mode with the largest magnitude of c_α for a given configuration, leading to the *maximal mode* projection. In all these situations the key is that the formulation of the friction we are using keeps the individual molecular pieces of the dynamic solvent response remaining in plain sight, ready to be incorporated or deliberately frozen out, as we desire.

III. NUMERICAL METHODS

A. Model system and simulation details

In order to obtain sets of Boltzmann-distributed liquid configurations and to have some exact dynamical results to compare with, we carried out several constant number-volume-energy (NVE) molecular dynamics simulations for a single rigid diatomic dissolved in 106 solvent atoms. Lennard-Jones (LJ) potentials

$$u(r)=4\varepsilon[(\sigma/r)^{12}-(\sigma/r)^6], \tag{3.1}$$

were used to model the interactions between all the atoms in the system, including those of the diatomic. The total potential was thus of the form

$$V=\sum_{A=a,b}\sum_{j=1}^{N}u_{uv}(r_{Aj})+\sum_{\substack{j,k=1\\ k>j}}^{N}u_{vv}(r_{jk}), \tag{3.2}$$

where *uv* and *vv* refer to the solute–solvent and the solvent–solvent interactions, respectively, A labels the two sites of the diatomic, and j and k are the solvent-atom indices. As in many of the previous studies of vibrational relaxation in atomic solvents,[26,27] we set the mass, m_u, of each atom in the solute identical to those of the solvent, m_v, and we chose the $u_{uv}(r)$ and $u_{vv}(r)$ potentials to be identical ($\varepsilon_{uv}=\varepsilon_{vv}=\varepsilon$, $\sigma_{uv}=\sigma_{vv}=\sigma$). Argon-type parameters,

$$\sigma = 3.405\,\text{Å}, \quad \varepsilon/k_B = 119.8\,\text{K}, \quad m_{\text{Ar}} = 40\ \text{a.m.u.}, \tag{3.3}$$

were used to translate our numerical results into experimental units.

The results presented here were obtained for five different solute bond lengths, $d=1.25\sigma$, 0.65σ, 0.325σ, 0.16σ, and 0.08σ, corresponding to an excluded volume for the diatomic of $V_{\text{vdW}}/\text{Å}^3 = 41.4$, 38.0, 30.4, 25.6, and 23.3, respectively.[28] Our default thermodynamic state was the high density, room-temperature supercritical fluid state ($\rho\sigma^3=1.05$ and $k_BT/\varepsilon=2.5$) frequently used for studying vibrational relaxation,[26,27] though we also conducted some liquid state ($\rho\sigma^3=0.8$, $k_BT/\varepsilon=1.0$) simulations for comparison purposes.

The simulations themselves[29] employed standard periodic boundary conditions and minimum image conventions. In each case, the system was initially started from an fcc lattice, with a transnational order parameter used to monitor equilibration to a fluid state. To propagate the positions of the solvent atoms and the center of mass of the diatomic, we used the velocity-Verlet algorithm with a timestep, $dt=0.001\tau_{\text{LJ}}$, where $\tau_{\text{LJ}}(=\sqrt{m_{\text{Ar}}\sigma^2/\varepsilon})$ for argon is 2.16 ps. The reorientational motion of the diatomic, though, was integrated using a velocity version of the algorithm proposed by Fincham[30] (Appendix A). Angular-velocity and torque autocorrelation functions were calculated by running 10 000 molecular dynamics (MD) trajectories with a length of 2000 timesteps each.

B. Calculation of influence spectra

To compute the influence spectra, we collected liquid configurations along a molecular dynamics trajectory at 50-time-step intervals (chosen so as to minimize correlation between the adjacent configurations sampled). At each of the 40 000 configurations generated in this fashion, the dynamical matrix, **D**, was constructed:

$$D_{j\mu,k\nu} = \frac{1}{\sqrt{m_j m_k}} \frac{\partial^2 V}{\partial r_{j\mu}\partial r_{k\nu}}, \tag{3.4}$$

with j and $k=0$, ..., N, the atomic and solute-center-of-mass indices, and μ and ν labeling the x, y, and z directions. The eigenvalues, ω_α^2, and eigenvectors, $U_{j\mu,\alpha}$, of the dynamical matrix were then evaluated numerically using standard methods (conversion of the dynamical matrix to a tridiagonal matrix followed by application of the QL method for diagonalization).[31] To produce the untransformed rotational coupling constants

$$c_{j\mu} = (1/\sqrt{m_j})(\partial N/\partial r_{j\mu}) = -(1/\sqrt{m_j})(\partial^2 V/\partial\theta\partial r_{j\mu}), \tag{3.5}$$

we used the working formula,

$$c_{j\mu} = -\frac{d}{\sqrt{m_j}} \sum_{A=a,b} \sum_{j=1}^{N} f_A[\overleftrightarrow{t}_{uv}(\vec{r}_{Aj})\cdot\hat{\beta}]_\mu \quad (j=0)$$

$$= \frac{d}{\sqrt{m_j}} \sum_{A=a,b} f_A[\overleftrightarrow{t}_{uv}(\vec{r}_{Aj})\cdot\hat{\beta}]_\mu \quad (j\geqslant 1), \tag{3.6}$$

where $\hat{\beta}=(\cos\theta\cos\phi, \cos\theta\sin\phi, -\sin\theta)$, and the f_A are $-\frac{1}{2}$ and $\frac{1}{2}$ for $A=a$ and b, respectively. Here we have defined the interatomic ''spring-constant'' tensor, $\overleftrightarrow{t}_{uv}(\vec{r})$, as

$$\overleftrightarrow{t}_{uv}(\vec{r}) = u''_{uv}(r)\hat{r}\hat{r} + [u'_{uv}(r)/r][\overleftrightarrow{1} - \hat{r}\hat{r}], \tag{3.7}$$

where the unit vector $\hat{r}=\vec{r}/r$, and the primes denote derivatives with respect to r. The transformed coupling strengths, c_α, were then evaluated from Eq. (2.13). With the mode frequencies and these coupling constants in hand, the rotational friction spectrum for each configuration could be computed from Eq. (2.3) and the results averaged over all 40 000 configurations. To check for finite-size effects, we also calculated the friction spectra using 30 and 254 solvent atoms, with results virtually identical to those from the 106-solvent-atom calculations. The final ingredient in the rotational GLE, the rms-librational frequency, $\overline{\Omega}$

$$\overline{\Omega}^2 = \left\langle \sum_{A=a,b} \sum_{j=1}^{N} (f_A d)[(f_A d)(\hat{\beta}\cdot\overleftrightarrow{t}_{uv}(\vec{r}_{Aj})\cdot\hat{\beta}) - u'_{uv}(r_{Aj})(\hat{r}_{Aj}\cdot\hat{e})] \right\rangle, \tag{3.8}$$

was calculated by averaging over 10^6 configurations.

Even after being averaged over 40 000 configurations, our friction spectra are rather noisy in the high-frequency region. The reasons for this behavior are, in fact, rather fundamental reflections of the few-body mechanism by which a liquid responds at high frequency.[17,19,32–34] For our subsequent calculations of the time-and frequency-domain friction kernels, $\eta^{\text{INM}}(t)$ and $\tilde{\eta}^{\text{INM}}(\omega)$, we therefore fitted the friction spectra to the functional form

$$\rho_{\text{fric}}(\omega) = \sum_{k=1}^{N_{\text{Gauss}}} B_k\omega \exp\left[-\left(\frac{\omega - E_k}{G_k}\right)^2\right]. \tag{3.9}$$

The Levenberg–Marquardt method[35] was used to find the amplitude, B_k, center frequency, E_k, and width, G_k of each Gaussian. Both one ($N_{\text{Gauss}}=1$) and two ($N_{\text{Gauss}}=2$) Gaussian fits were examined, and the parameters so obtained are listed in Table I. The fitted spectra, plotted in Fig. 3, illustrate the excellent quality of the two-Gaussian fit in particular.

Finally, to place our results for the rotational friction spectra in context, we also calculated what the corresponding influence spectra would have been for vibrational relaxation and solvation taking place in the same system. The vibrational friction spectra was obtained based on Eq. (2.11), assuming the diatomic could translate but not rotate. The vibrational coupling constants necessary for this spectrum, $c_{j\mu}=-(1/\sqrt{m_j})(\partial^2 V/\partial x\partial r_{j\mu})$, with $x=|\vec{r}_b-\vec{r}_a|$ the distance between the two atoms on the diatomic, were calculated

TABLE I. Rotational friction spectra for a homonuclear diatomic dissolved in a dense supercritical argon fluid.

Bond length	$(N_{\text{Gauss}})^a$	$B_k(10^{-21}\text{ J})$	$E_k(\text{cm}^{-1})$	$G_k(\text{cm}^{-1})$	Rel. dev.[b]
1.25σ	2	654.2	94.2	75.5	0.052
		240.4	148.3	47.1	
	1	791.4	111.5	72.2	0.10
0.65σ	2	120.0	84.1	76.8	0.059
		67.0	144.8	48.1	
	1	156.2	110.7	72.8	0.11
0.325σ	2	15.7	77.1	68.4	0.063
		13.5	139.0	53.3	
	1	23.6	110.5	70.3	0.12
0.16σ	2	1.49	81.7	88.4	0.079
		1.08	128.5	55.2	
	1	2.37	108.8	72.6	0.092
0.08σ	2	0.135	80.9	66.2	0.064
		0.1	140.2	51.1	
	1	0.19	109.0	70.1	0.099

[a]Number of Gaussians used for each fit of the rotational friction spectrum: $\rho_{\text{fric}}(\omega)=\Sigma_{k=1}^{N_{\text{Gauss}}}B_k\omega\exp[-((\omega-E_k)/G_k)^2]$.
[b]Relative deviation of the fitted spectrum from the simulated spectrum: $\int d\omega|\rho_{\text{fit}}(\omega)-\rho_{\text{data}}(\omega)|/\int d\omega\,\rho_{\text{data}}(\omega)$.

from expressions we have reported previously.[22] To evaluate the solvation spectrum using Eq. (2.12), we assumed, as with the ε model of Stephens, Saven, and Skinner,[36] that the interactions between atoms in the ground, u_g, and the excited, u_e, states were LJ potentials differing only in well depth, so that

$$v(r_{0j})=u_e(r_{0j})-u_g(r_{0j})=4\varepsilon\lambda[(\sigma/r_{0j})^{12}-(\sigma/r_{0j})^6]. \tag{3.10}$$

The constant λ was set equal to 0.1.[17]

IV. RESULTS

A. Universal features of influence spectra

Our arguments in Sec. II suggest that the ways in which a solvent sees the rotational motion of a solute could be significantly different from how it senses the vibrational motion, or *a fortiori*, how it sees differences in electronic states,

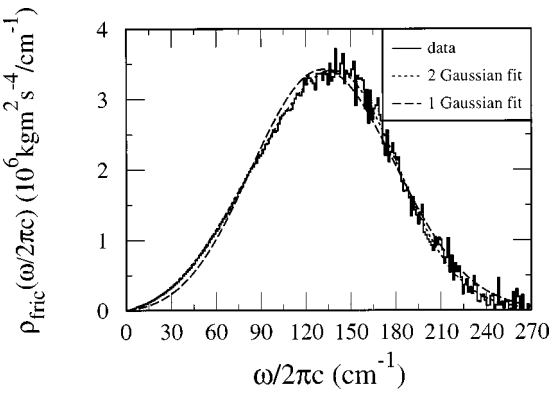

FIG. 3. An example showing two different fits to a calculated rotational friction spectrum. The system shown is a diatomic with bond length of 1.25σ dissolved in dense supercritical argon ($\rho\sigma^3=1.05$, $k_BT/\epsilon=2.5$).

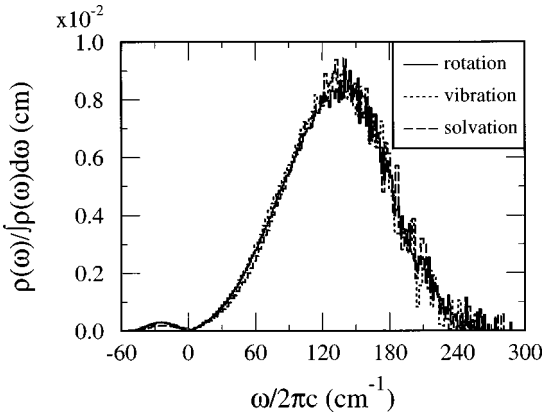

FIG. 4. Normalized influence spectra for different relaxation processes of a homonuclear diatomic solute dissolved in dense supercritical argon. The rotational friction, vibrational friction, and solvation spectra are drawn as solid, short-dashed, and long-dashed lines, respectively. The details of the models used are presented in Sec. III. The solvation spectrum is taken from Ref. 17, and, as usual, imaginary frequencies are plotted as negative frequencies.

in the same solute. Comparing Eqs. (2.10) and (2.11), for example, might lead one to guess that motion of the solvent perpendicular to the solute bond is critical in the former, whereas motion parallel to the bond is key in the latter—and that the dynamics of solvation, Eq. (2.12), would be completely unrelated. What we find, however, is quite different. In fact there is a striking universality to solvent influence spectra, independently of whether one looks at rotational relaxation, vibrational relaxation, or solvation. Figure 4 shows that, when normalized, these three influence spectra are indistinguishable from one another for our model system. Evidently, aside from constant scaling factors, the solvent's instantaneous normal modes interact in precisely the same way with these three rather different physical processes.

The microscopic origin of the similarity between the solvation and the vibrational friction spectra has, in fact, already been emphasized several times,[17,19,34] though an explanation has only been offered for the commonalities seen in the high frequency part of the response. The idea is that for any short-ranged, sharply varying spectroscopic probe, whether it involves forces or potentials, the highest frequency part of the spectral response will come, almost entirely, from the small number of solvent molecules which are instantaneously closest to the solute. It is these most strongly interacting partners, moving in ways determined solely by the geometry of the solvent about the solute, that govern all possible high-frequency solute relaxation processes. Indeed, the instantaneously nearest-neighbor solvent atoms by themselves are responsible for a significant fraction of both the solvation (82%) and the vibrational friction (65%) spectra in this model.[17] The high-frequency universality of vibrational relaxation and solvation clearly suggests that the solute's response to these nearest few atoms is remarkably insensitive to the specific functional form of the external probe. What we can do now is to use our new example of rotational relaxation to explore the generality of this analysis of the high-frequency response—and to see to what extent the universality continues to extend to lower frequencies as well.

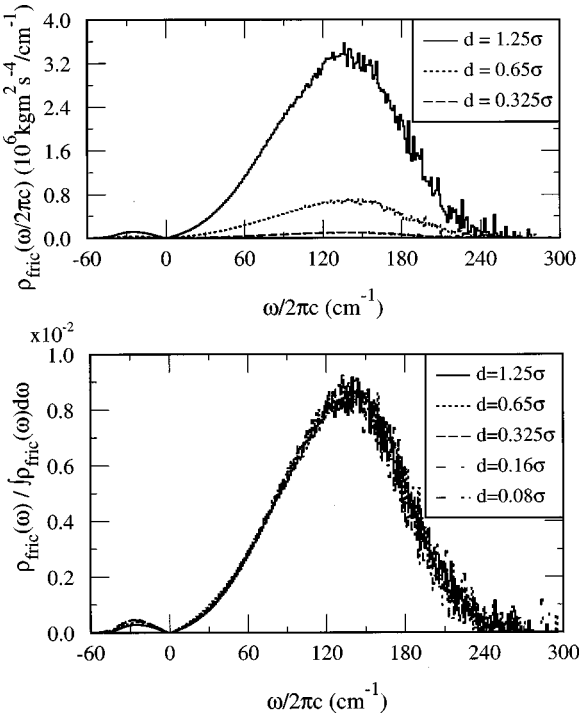

FIG. 5. The effect of solute bond length on the rotational friction spectrum of a homonuclear diatomic dissolved in dense supercritical argon. The top panel presents the actual rotational friction spectra for three different bond lengths, d, making clear the sizeable differences in coupling strengths. By way of contrast, the normalized rotational friction spectra for five different bond lengths are shown in the bottom panel.

Consider, for example, the effect on rotational friction of changing the solute size, Fig. 5. Modifying the bond length presumably ought to have a noticeable effect on the local solute–solvent geometry. Indeed, as the diatomic gets shorter, the coupling to the solvent is significantly reduced, resulting in the smaller absolute magnitudes for the friction. In much the same way, the rms- librational frequency, $\bar{\Omega}$, systematically shrinks as the solute does, indicating the reduced static caging abilities of the solvent (Table II). The bottom panel of Fig. 5 reveals, however, that the rotational friction spectra have an identical shape for all five bond lengths: altering the solute size has no effect on the spectra beyond a simple scaling of overall magnitudes.

In retrospect, this kind of outcome is just what we should have expected from the solvent–solute coupling being filtered through a few special neighbors of the solute. While the geometry of the first solvent shell around the solute is going to be noticeably changed by diminishing the bond length, the geometry of a single nearby solvent atom *around a single solute site* is not. The few-body character of the dynamical coupling to the solute appears not only to be universal but to operate at the level of individual solute sites.

TABLE II. Instantaneous-librational frequencies, $\bar{\Omega}$, for a homonuclear diatomic dissolved in a dense supercritical argon fluid.[a]

Band length	1.25σ	0.65σ	0.325σ	0.16σ	0.08σ
$\bar{\Omega}/2\pi c$(cm^{-1})	75.87	66.34	50.74	32.68	17.84

[a]Reported as the root-mean-square average defined by Eq. (2.8).

TABLE III. Rotational and vibrational coupling strengths for a homonuclear diatomic dissolved in a supercritical argon fluid.

Bond length	Relaxation process	C[a] (10^6 kgm^2 s^{-4})	$R(\parallel)$[b] (%)	$R(\perp)$ (%)	$R(L)$ (%)	$R(T)$ (%)
1.25σ	rot	393	26.9	73.1	64.4	34.5
	vib	328	36.3	63.7	84.5	15.6
0.65σ	rot	82.2	19.6	80.4	87.2	11.7
	vib	62.9	48.8	51.2	93.3	6.0
0.325σ	rot	11.7	26.6	73.4	94.9	4.2
	vib	13.8	55.3	44.7	95.9	3.4
0.16σ	rot	1.15	34.8	65.2	96.6	2.6
	vib	2.05	61.0	39.0	97.5	1.9
0.08σ	rot	9.23×10^{-2}	39.1	60.9	96.8	2.3
	vib	0.20	63.8	36.2	98.0	1.5

[a]Total coupling strength derived from the rotational friction spectrum (rot) and from the vibrational friction spectrum (vib). The vibrational coupling reported here is multiplied by the bond length squared, d^2.

[b]The percentages R denote the fraction of the total coupling corresponding to different kinds of solvent motion. In particular, $R(\parallel)$, $R(\perp)$, $R(L)$, and $R(T)$ give the ratios of the areas under the parallel, perpendicular, longitudinal, and transverse projected friction spectra (respectively) to the area under the total friction spectrum.

B. Specific dynamical mechanisms for rotational and vibrational friction

If the dynamical coupling between the solute and the solvent is really that well defined, it should be possible to elucidate actual mechanisms for rotational and vibrational relaxation. So, just what kinds of solvent motions are going to be most effective in causing rotational and vibrational friction? If our remarks in the proceeding section are to be taken seriously, the first step might be to project the friction spectra into contributions from solvent motions *parallel* and *perpendicular* to the bond axis.[22] Table III lists the resulting values of C, the total coupling strengths underlying the rotational and vibrational friction, for our five bond lengths. [The total coupling strength of each projection, $C(\text{proj}) = \langle \Sigma_\alpha (c_\alpha^{\text{proj}})^2 \rangle$, is defined as the area under the projected spectrum, so the ratio $R(\text{proj}) = C(\text{proj})/C$ measures the contribution from each projection to the total friction.] We note from the table that perpendicular motion really is central to the rotational friction, with components ranging from 60% to 80% of the friction spectra. Some of this dominance of the perpendicular motion is trivial geometry; in three dimensions one expects a 33.3% parallel and a 66.7% perpendicular contribution on purely statistical grounds. But, as can be seen in Table III, except for the two shortest bond lengths, the perpendicular dominance goes beyond statistical expectations. The perpendicular projection reaches a maximum at $d = 0.65\sigma$ and decreases as the bond length is shortened.

The relevance of these numbers become more convincing if we compare this behavior to that seen with vibrational friction (Table III). Here we see that the friction is mainly controlled by parallel motions of the solvent atoms, especially for short bond lengths. The parallel projection is just

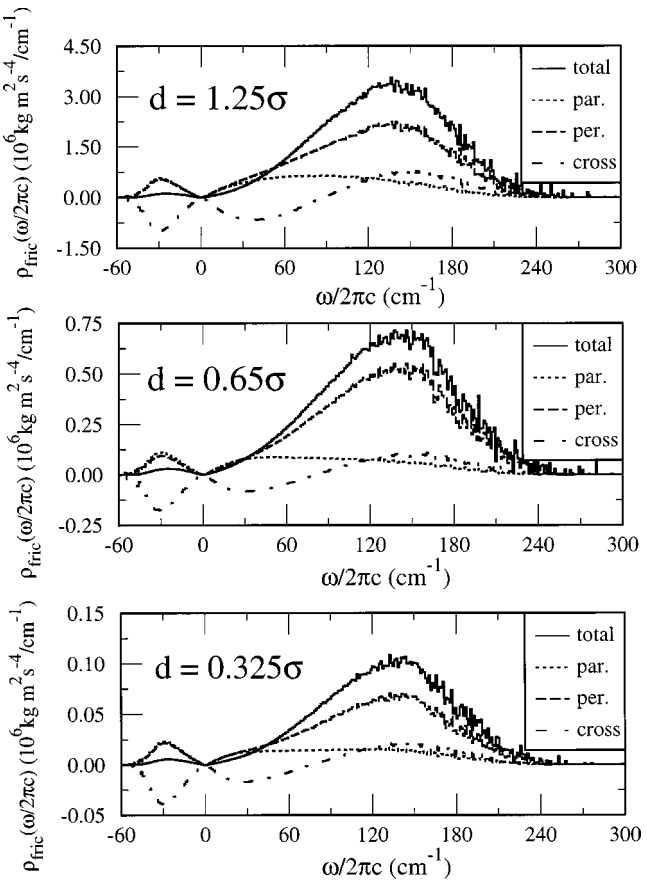

FIG. 6. The contributions of different kinds of solvent motion to the rotational friction felt by a homonuclear diatomic dissolved in dense supercritical argon. Shown here are the parallel (par.), perpendicular (per.), and coupled (cross) projections of the rotational friction spectrum plotted for three different solute bond lengths: $d=1.25\sigma$, 0.65σ, and 0.325σ.

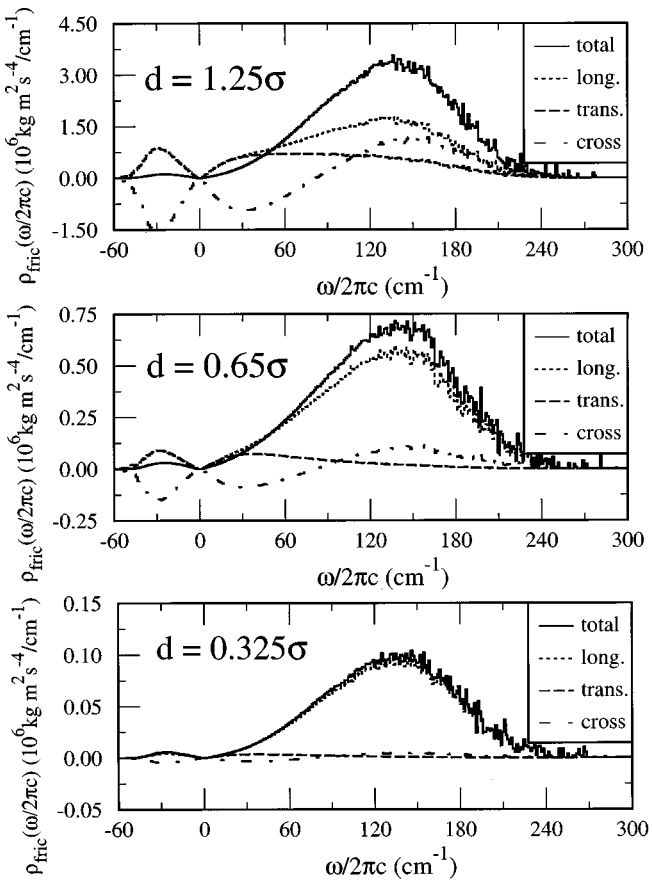

FIG. 7. The contributions of different kinds of solvent motion to the rotational friction felt by a homonuclear diatomic dissolved in dense supercritical argon. Shown here are the longitudinal (long.), transverse (trans.), and cross projections of the rotational friction spectrum plotted for three different solute bond lengths, $d=1.25\sigma$, 0.65σ, and 0.325σ.

above 33% for 1.25σ, the longest bond length, but when the bond length is decreased to 0.65σ, it jumps to 50% of the total friction. Further decreasing the bond length increases the parallel contribution to 64%, almost double its expected statistical weight. Vibrational and rotational relaxation evidently do seem to rely on geometrically distinct solvent motions.

This argument to this point is based solely on the total coupling strength of each projection, but it is worth noting that the relative importance of a given kind of motion depend reasonably strongly on the frequency one is probing. In Fig. 6 we plot the rotational friction spectra, $\rho_{\mathrm{fric}}(\omega)$, for several solute bond lengths with the components from parallel and perpendicular solvent motions projected out. For imaginary frequencies and for the lowest real frequencies ($\leqslant 30\ \mathrm{cm}^{-1}$), the parallel and perpendicular motions are actually comparable, with significant cross contributions. But as the frequency increases, the perpendicular projection takes over. This kind of frequency dependence is common to all three of the spectra displayed in Fig. 6, suggesting that the mechanisms by which the lowest frequency INMs modulate solute relaxation may have somewhat different geometrical features than the few-body coupling favored by the higher-frequency modes.

It is interesting to contrast these parallel/perpendicular signatures of relaxation with alternative dynamical possibilities for the solvent. Rather than studying the preferred orientations of the solvent motion with respect to the solute bond axis, for example, we can look at how the dynamical efficiency varies with orientation with respect to the solute center of mass. Solvent momenta parallel and perpendicular to the vector between the solvent and the solute center of mass we shall call *longitudinal* and *transverse* motions, respectively.[22] It is plain from Table III that, regardless of the bond length, longitudinal motion is always the major source of both rotational and vibrational friction. We can see this behavior in a little more detail in Fig. 7, where we show these longitudinal-transverse projections of the rotational friction spectrum for a number of different bond lengths. As in the parallel-perpendicular projection, the longitudinal motion is barely distinguishable from the transverse motion for the lowest real frequencies (and for imaginary frequencies), but it completely dominates the remainder of the influence spectrum. In fact for the smallest bond length shown, $d=0.325\sigma$, the longitudinal projection reproduces the full spectrum almost quantitatively.

It is certainly true that there are some quantitative differences between the longitudinal projections for the rotational and vibrational frictions, but even these distinctions become smaller as the bond length diminishes. The significant point

TABLE IV. Few-body contributions to the rotational and vibrational friction on a diatomic dissolved in a dense supercritical argon fluid.

Bond length	Relaxation process[a]	R (max. mode) (%)[b]	R (nearest) (%)	R (max. atom) (%)[c]	# of max. atoms[d]
1.25σ	rot	39.4	71.5	88.3	10.3
	vib	38.0	74.6	90.4	10.1
0.65σ	rot	41.7	75.9	91.4	9.0
	vib	41.0	79.0	95.3	9.4
0.325σ	rot	42.1	80.1	94.4	8.3
	vib	42.1	83.5	98.6	8.3
0.16σ	rot	41.7	82.3	96.3	7.9
	vib	43.3	85.2	100.8	7.6
0.08σ	rot	42.1	81.0	96.3	7.7
	vib	43.6	83.5	101.7	7.2

[a]Projections of the rotational (rot) and vibrational (vib) friction spectra, respectively.

[b]The percentages R denote the fractions of the total solute-solvent coupling corresponding to different kinds of solvent involvement (computed as the ratio of the area under each projected spectrum to the area under the total friction spectrum). In particular R (max. mode) is the fractional contribution from the maximally contributing solvent mode, R (nearest) gives the contribution from the solvent atom nearest the solute and R (max. atom) gives the total contribution of the solvent atoms which have the largest coupling magnitude in any of the solvent modes.

[c]Because of the presence of small, negative contributions from the cross terms, individual projections can actually be slightly more than 100% on occasion. See Ref. 38.

[d]The average numbers of the maximally coupled atoms (as described in footnote b) in a single liquid configuration.

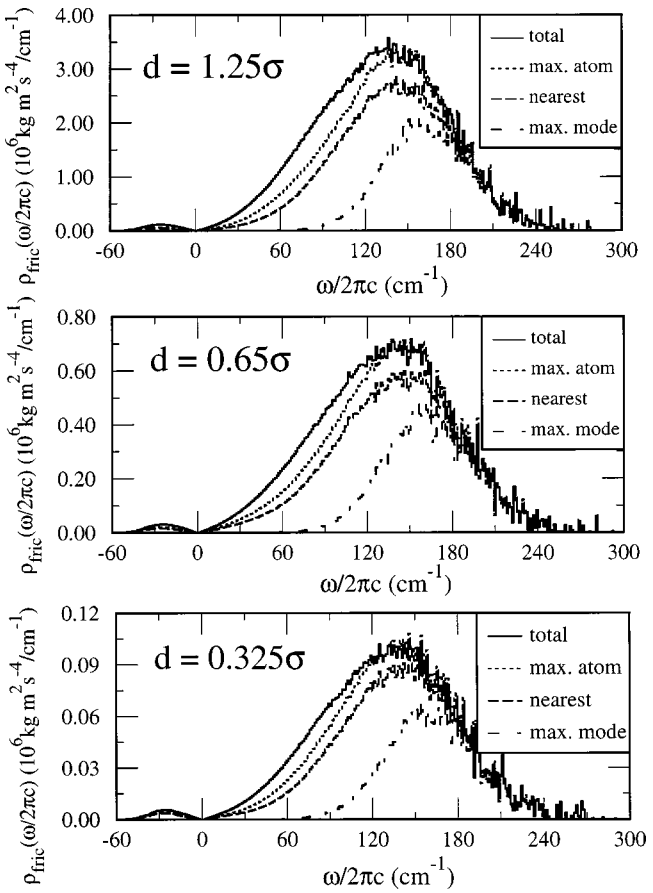

FIG. 8. Few-degree-of-freedom projections of the rotational friction spectra for a homonuclear diatomic dissolved in dense supercritical argon. The contributions of the single instantaneous normal mode with the largest coupling (max. mode), the single solvent atom closest to the solute (nearest), and the solvent atoms which make the largest contribution to the coupling of the solvent modes (max. atom) are plotted for three different solute bond lengths, $d=1.25\sigma$, 0.65σ, and 0.325σ.

here is that in this model rotational and vibrational relaxation are largely alike in being promoted by solvents moving *towards* the solute. This result is obviously not entirely unexpected, but it is not quite as trivial as it might appear. We have found that this simple finding tends not to be as clearcut with more complicated molecular solvents, and one could certainly envision examples in which dipolar forces were sufficiently important that the transverse solvent motions could play a real role. Our present study with atomic solvents may serve as a useful point of comparison when such cases do arise.

C. Few-body features of the friction spectra

We turn now from the question of how the solvent can move to foster solute relaxation to the question of which solvents are doing the moving. Specifically we want to focus on the particular solvent atoms and the instantaneous normal modes most strongly correlated with the solute relaxation. A *maximal mode* projection, which selects, for each configuration, the mode with the largest coupling strength,[17] shows that a single mode accounts (in an average sense) for about 40% of the total coupling strength (Table IV). This figure is deceiving, however. On frequency resolving this projection, Fig. 8, we see that it exactly matches the high frequency part of the full influence spectra ($\omega/2\pi c \geqslant 160\,\mathrm{cm}^{-1}$). Evidently it is a single mode out of the macroscopic total number of modes that matters in the high-frequency part of the rotational friction. This same maximal mode projection, however, is rather poor at emulating the bottom half of the spectra.

A similar perspective is obtained when we consider the solvent atoms which are the *nearest neighbors* of the solute.[17,37] These nearest-neighbor contributions (Table IV) account for a more respectable 72% to 82% of the rotational friction spectrum, but, once again, the projection precisely replicates the high-frequency wings of the spectra (Fig. 8). The nearest-neighbor projection tends to match the full spectra over a broader frequency range than the maximal mode projection, but it still misses a significant portion of the full spectra at low frequencies.

It is only when we realize that the nearest neighbors will not necessarily lead to the largest couplings that we get closer to a quantitative picture of the relaxation mechanism. If we project out from each mode the contribution of the single atom with the largest coupling strength (Table IV), we find some impressive figures. This *maximal atom* projection generates from 88% to 96% of the rotational friction and 90% to 100% of the vibrational friction.[17,19,38] Because for a given configuration the identity of the maximally contributing atom varies from mode to mode, we are actually seeing

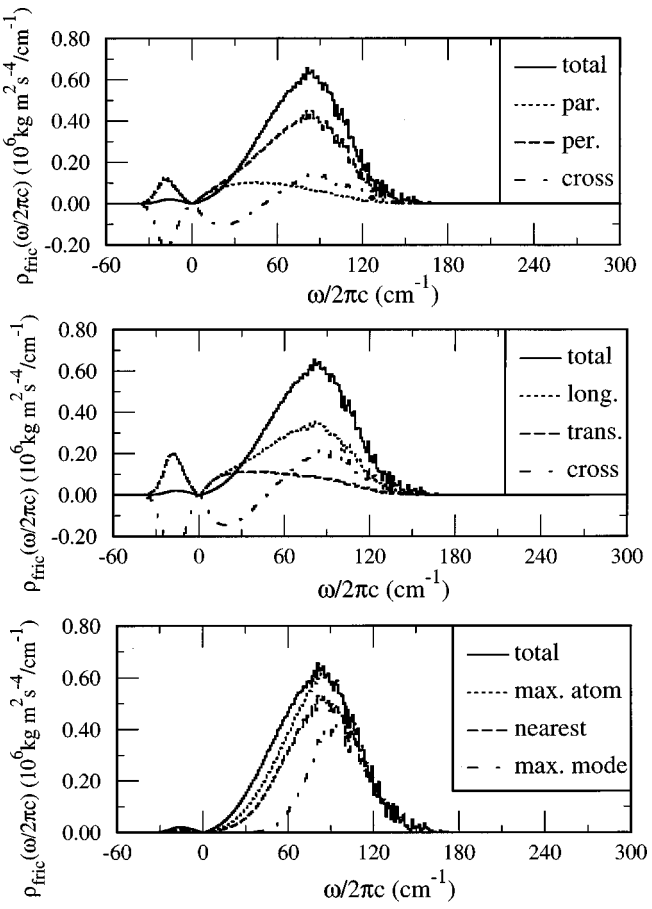

FIG. 9. Different solvent contributions to the rotational friction for a homonuclear diatomic dissolved in *liquid* argon ($k_BT/\epsilon=1.0$, $\rho\sigma^3=0.8$). Drawn in the figure are the parallel–perpendicular (par.–per.), longitudinal–transverse (long.–trans.), maximally coupled solvent mode (max. mode), nearest-solvent neighbor (nearest), and maximally coupled solvent atom (max. atom) projections of the rotational friction spectrum for a solute with bond length $d=1.25\sigma$.

the contributions of several different atoms; the average numbers of which are also listed in Table IV. As the bond length is shortened, the median number of these maximally coupled atoms recedes slightly, from around 10 to 7. Of course, the size of the first solvation shell will also vary as we change the solute size, but the correlation with this coordination number is surprisingly weak.[39] What one can say is that these median numbers tend to reflect little more than half of the first solvent shell—still a microscopic number. On the balance what we can see from Fig. 8 is that we capture the vast majority of the ways in which the solvent contributes to rotational relaxation by focusing on just these few maximally coupled atoms, though we apparently need more than this tiny number of solvents to capture the essence of the lowest frequency instantaneous friction.

Somewhat more globally, one can point to several features common to all of these few-body projections. First, all of them reproduce the high-frequency parts of the friction spectra, and they do so with quantitative accuracy. Second, in contrast to the directional projections, these more local projections are insensitive to changes in the solute geometry. With decreasing bond length, the perpendicular projection of the rotational friction varies nonmonotonically between 60% and 80% while the longitudinal projection monotonically increases from 64% to 97% of the total friction. By contrast, the maximal-mode (39% to 42%), nearest-neighbor (72% to 82%), and maximal-atom (88% to 96%) projections are all relatively invariant to the changes in the solute size. The third, and most crucial point, though, is that, as shown in Table IV, these few-body projections end up with nearly the same fractions for both rotational and vibrational relaxation, though the vibrational relaxation numbers are almost always a few percent higher. It is difficult to avoid drawing the conclusion that the universality of the influence spectra we saw in Figs. 4 and 5 is a reflection of the overriding importance of few-body dynamics.[17,19,32–34]

TABLE V. Rotational and vibrational coupling strengths for a homonuclear diatomic dissolved in liquid argon.

Bond length	Relaxation process	C[a] (10^6 kgm^2 s^{-4})	$R(\|\|)$[b] (%)	$R(\perp)$ (%)	$R(L)$ (%)	$R(T)$ (%)
1.25σ	rot	43.4	24.1	75.9	68.2	31.1
	vib	33.8	38.1	61.9	86.8	13.2
0.65σ	rot	9.9	18.9	81.7	88.7	10.4
	vib	7.5	50.2	49.8	94.4	5.2
0.325σ	rot	1.5	25.8	74.2	95.5	3.7
	vib	1.8	55.9	44.1	96.6	2.9

[a]Total coupling strength derived from the rotational friction spectrum (rot) and from the vibrational friction spectrum (vib). The vibrational coupling reported here is multiplied by the bond length squared, d^2.

[b]The percentages R denote the fraction of the total coupling corresponding to different kinds of solvent motion. In particular, $R(\|)$, $R(\perp)$, $R(L)$, and $R(T)$ give the ratios of the areas under the parallel, perpendicular, longitudinal, and transverse projected friction spectra (respectively) to the area under the total friction spectrum.

As a final matter, we should note that we have presented all of our analysis based on a single thermodynamic state. To see how the conclusions drawn from the dense supercritical fluid would change with thermodynamic conditions, we repeated the INM analysis for a true liquid-state point ($k_BT/\epsilon=1.0$ and $\rho\sigma^3=0.8$) for three different solute bond lengths, $d/\sigma=1.25,0.65,0.325$. In Fig. 9, we plot all of the same projected spectra we looked at before, but for the liquid solvent and for the one case $d=1.25\sigma$. There is, in fact, a noticeable change: the frequency range spanned by INMs is reduced by nearly half in both the real and imaginary frequencies. The qualitative behaviors of the various projections, though, remain intact, and the proportions of each projection listed in Tables V and VI remain in quantitative agreement with those from the supercritical fluid.

V. CONCLUDING REMARKS

There is very little in the prevailing hydrodynamic models of rotational relaxation which would have led us to suspect that rotational dynamics would have anything in common with vibrational population relaxation. From an experimental standpoint, rotational relaxation and rotational diffusion have almost become synonomous terms in the treatment of reorientation in liquids. That similar kinds of

TABLE VI. Few-body contributions to the rotational and vibrational friction on a diatomic dissolved in liquid argon.

Bond length	Relaxation process[a]	R (max. mode) (%)[b]	R (nearest) (%)	R (max. atom) (%)[c]	# of max. atoms[d]
1.25σ	rot	46.8	74.4	90.1	11.0
	vib	46.0	77.6	92.3	11.3
0.65σ	rot	49.0	78.2	92.5	9.6
	vib	48.5	80.8	96.3	10.5
0.325σ	rot	48.5	80.5	94.7	8.6
	vib	48.9	83.7	98.6	8.9

[a]Projections of the rotational (rot) and vibrational (vib) friction spectra, respectively.

[b]The percentages R denote the fractions of the total solute-solvent coupling corresponding to different kinds of solvent involvement (computed as the ratio of the area under each projected spectrum to the area under the total friction spectrum). In particular R (max. mode) is the fractional contribution from the maximally contributing solvent mode, R (nearest) gives the contribution from the solvent atom nearest the solute and R (max. atom) gives the total contribution of the solvent atoms which have the largest coupling magnitude in any of the solvent modes.

[c]Because of the presence of finite, though small, negative contributions from the cross terms, individual projections can actually be slightly more than 100% on occasion.

[d]The average numbers of the maximally coupled atoms (as described in footnote b) in a single liquid configuration.

non-diffusive, few-body solvent motions would come into play in both rotation and vibrational relaxation makes the connection especially intriguing.[40]

The instantaneous perspective, though, makes it clear that not only rotation and vibration, but solvation are triggered by a spectrum of solvent motions virtually identical to one another. There are still some detailed geometrical differences: solvents moving perpendicular to the solute bond axis are best at promoting rotational relaxation, for example, whereas motion parallel to the bond axis is best for fostering vibrational relaxation, but, for the most part, the relaxation processes for our nonpolar solute dissolved in our nonpolar solvent seem to be remarkably universal. Both rotational and vibrational friction are largely governed by the longitudinal motion of solvent atoms towards the center of the solute. Much more strikingly, both kinds of friction are dominated by the motions of a miniscule number of solvents. Unlike the geometrical considerations, which depend to a varying extent on the size and shape of the solute, the few-body character is as close to an invariant as one could imagine. Just one or two atoms in the vicinity of the solute contribute more than 70% of the friction spectra, and no more than 10 atoms is ever needed to reproduce the friction at 90% level. It is undoubtedly this few-body flavor of the solvent friction that lies behind most of the universality we see in the influence spectra for different physical processes and the distinct solute sizes.

These results, nonetheless, do pose a number of questions. Most obvious of these is what happens to our findings when we go to more complicated molecular solvents. Although the pronounced few-body signatures found in recent INM analyses of vibrational relaxation in molecular fluids are suggestive, it remains to be seen how, or if, rotational dynamics changes when we shift from atoms to molecules as solvents. One can also begin to ponder some extra dynamical possibilities opened by molecular solvents. What determines how much of a solute's energy initially goes to solvent rotation and how much to solvent translation? Are either the few-body character or the similarity between vibrational and rotational relaxation altered significantly when the solute–solvent interaction becomes long ranged?

This last question is essentially the issue of dielectric friction, usually defined implicitly as the excess friction accompanying the electrostatic forces in the system.[3,13,14,41] The concept has been central to much of the discussion of rotational dynamics in polar liquids, yet the recent careful experimental study of Horng, Gardecki, and Maroncelli[8] has raised the question of just how complete our picture of it is. The excess friction caused by Coulombic forces can be quite significant, but our and other workers' observations in studying vibrational relaxation were that the real effects of these forces could be rather indirect.[14,42–44] In our own study,[19,42] we noted that if the solute-solvent interaction could be written as a sum of ''mechanical'' and electrostatic potentials,

$$u_{uv}(r) = u_{\mathrm{mech}}(r) + u_{\mathrm{elec}}(r), \tag{5.1}$$

we could rigorously divide the instantaneous friction into the mechanical, $\rho^{\mathrm{mech}}(\omega)$, dielectric, $\rho^{\mathrm{diel}}(\omega)$, and cross, $\rho^{\mathrm{cross}}(\omega)$, terms

$$\rho(\omega) = \rho^{\mathrm{mech}}(\omega) + \rho^{\mathrm{diel}}(\omega) + \rho^{\mathrm{cross}}(\omega) \tag{5.2}$$

(as opposed to the more common expression without the cross term). While it was tempting to identify the purely dielectric term here as the dielectric friction, the cross term was often found to be of similar magnitude and opposite sign. The direct dielectric effects were thus largely cancelled. Electrostriction, however, inevitably served to amplify the mechanical friction: electrostatic interactions made the local structure around the solute more compact, thereby enhancing the effects of the short-ranged forces.[42] It is worth noting then, that in this vibrational case the key to understanding the role of dielectric friction was having a theory sufficiently microscopic that we could tease out these kinds of coupled processes. We might anticipate that unraveling the molecular contributions to dielectric rotational friction could now be carried out similarly.

We should probably also remind the reader that, as we emphasized in the Introduction, we have not even tried to come to grips with the diffusive time scales of rotational motion. We were interested, instead, in the triggering motions that define the mechanisms by which relaxation takes place in a solvent. However, it is revealing to note that there are some connections with theories for the rotational diffusion. Gordon's classic m- and J-diffusion models, for example,[45] are concerned, for the most part, with a limit completely opposite from ours. By keeping $\sin\theta$ fixed in our formulation of the twist angles, Eq. (2.19) of paper I,[11] we are assuming that bond axis of our solute moves relatively little, so that the solute rotates smoothly, without tumbling, for each liquid configuration. Both the m- and J-diffusion models, by contrast, are based on significant random jumps in the direction of the angular momentum vector, followed by free rigid-body motion. Still, the J-diffusion model also

postulates that the magnitude of the angular momentum, J, randomly switches in such a way as to sample a Boltzmann distribution. Were we to interpret each successive jump as placing us in a new instantaneous liquid configuration, our approach too could be thought of as randomly choosing the magnitude of the solute angular momentum (and the orientation of the solute bond) from the Boltzmann distribution. The difference is that our ''jumps'' are much more infrequent and we attempt to treat the dynamics between our jumps much more accurately than simple, gas-phase, rigid-body motion would; the bond orientations and magnitudes of J we choose are only initial values in a subsequent trajectory calculation.[46]

This relationship with the J-diffusion model suggests that rotational dynamics might be uniquely suited as an example of how short-time, INM kinds of perspectives can be extended so as to include the onset of diffusive motion. The predominantly few-body character we see in the instantaneous dynamics could very well make the nature of this extension to the presumably collective behavior of diffusion all the more interesting.

ACKNOWLEDGMENTS

We thank Ross Larsen for sharing his insights and his data on solvation dynamics. We are also pleased to thank Ao Ma for helpful discussions. This work was supported by the National Science Foundation under Grant Nos. CHE-9417546, CHE-9625498, and CHE-9901095.

APPENDIX

For a rigid-linear molecule, Fincham[30] has proposed a leapfrog algorithm for propagation of the bond direction vector, $\hat{e}$, and its velocity, $\vec{u}=d\hat{e}/dt$. We derive here a velocity version of the algorithm for an improved performance in handling angular velocity and energy. The bond direction vector evolves in time as[47]

$$\dot{\hat{e}}=\vec{u}, \tag{A1}$$

$$\dot{\vec{u}}=(1/I)\vec{g}^{\perp}-|\vec{u}|^2\hat{e}, \tag{A2}$$

where $\vec{g}=\Sigma_A d_A \vec{F}_A$ is the so-called auxiliary torque on the molecule, $\vec{g}^{\perp}=\vec{g}-(\vec{g}\cdot\hat{e})\hat{e}$ is its component perpendicular to the bond axis. Here $\vec{F}_A$ is the force on site A of the linear top, and the distances d_A are defined as $\hat{e}\cdot(\vec{r}_A-\vec{r}_{\rm cm})$, where $\vec{r}_A$ and $\vec{r}_{\rm cm}$ are the site and center-of-mass positions of the linear top, respectively. The velocity-Verlet algorithm for the propagation of $\hat{e}$ and $\vec{u}$ from times t to $t+dt$ reads

$$\hat{e}(t+dt)=\hat{e}(t)+dt\,\vec{u}(t)+\tfrac{1}{2}(dt)^2\dot{\vec{u}}(t), \tag{A3}$$

$$\vec{u}(t+\tfrac{1}{2}dt)=\vec{u}(t)+\tfrac{1}{2}dt\,\dot{\vec{u}}(t), \tag{A4}$$

$$\vec{u}(t+dt)=\vec{u}(t+\tfrac{1}{2}dt)+\tfrac{1}{2}dt\,\dot{\vec{u}}(t+dt). \tag{A5}$$

Equations (A3) and (A4) are readily advanced in time by using $\dot{\vec{u}}(t)$ from Eq. (A2). To propagate Eq. (A5) however, we need the $|\vec{u}|^2$ at time $t+dt$, which is not available at that point. We thus need to evaluate $|\vec{u}(t+dt)|^2$ by making the approximation,

$$\dot{\vec{u}}(t+dt)\approx\frac{\vec{u}(t+dt)-\vec{u}(t+\frac{1}{2}dt)}{\frac{1}{2}dt}$$

$$=(1/I)\vec{g}^{\perp}(t+dt)-|\vec{u}(t+dt)|^2\hat{e}(t+dt), \tag{A6}$$

where Eq. (A2) has been used. Taking the dot product of Eq. (A6) with $\vec{e}(t+dt)$ gives

$$dt\,|\vec{u}(t+dt)|^2=2\vec{e}(t+dt)\cdot\vec{u}(t+\tfrac{1}{2}dt), \tag{A7}$$

where we have used the orthonormality of the bond direction vector ($\hat{e}\cdot\vec{g}^{\perp}=\hat{e}\cdot\vec{u}=0,\hat{e}\cdot\hat{e}=1$). This expression can be substituted into Eq. (A6) to give the desired $\dot{\vec{u}}(t+dt)$ and complete the final step of the propagation, Eq. (A5). The angular velocity, $\vec{\omega}(t)$, of the linear top can then be calculated as $\vec{\omega}(t)=\hat{e}(t)\times\vec{u}(t)$.

[1] D. Kivelson, in *Rotational Dynamics of Small and Macromolecules*, edited by Th. Dorfmuller and R. Pecora (Springer-Verlag, Berlin, 1987).
[2] B. J. Berne and R. Pecora, *Dynamic Light Scattering* (Robert E. Krieger, Malabar, 1990), Chap. 7.
[3] T. W. Nee and R. Zwanzig, J. Chem. Phys. **52**, 6353 (1970); M. Maroncelli, *ibid.* **106**, 1545 (1997).
[4] G. R. Fleming, *Chemical Applications of Ultrafast Spectroscopy* (Clarendon, Oxford, 1986), Chap. 6.
[5] D. S. Alavi and D. H. Waldeck, J. Chem. Phys. **94**, 6196 (1991); D. S. Alavi, R. S. Hartman, and D. H. Waldeck, *ibid.* **94**, 4509 (1991); D. S. Alavi and D. H. Waldeck, J. Phys. Chem. **95**, 4848 (1991); R. S. Hartman, D. S. Alavi, and D. H. Waldeck, *ibid.* **95**, 7872 (1991).
[6] G. S. Jas, Y. Wang, S. W. Pauls, C. K. Johnson, and K. Kuczera, J. Chem. Phys. **107**, 8800 (1997).
[7] J. S. Baskin, M. Gupta, M. Chachisvilis, and A. H. Zewail, Chem. Phys. Lett. **275**, 437 (1997); J. S. Baskin, M. Chachisvilis, M. Gupta, and A. H. Zewail, J. Phys. Chem. A **102**, 4158 (1998).
[8] M. L. Horng, J. A. Gardecki, and M. Maroncelli, J. Phys. Chem. A **101**, 1030 (1997).
[9] R. M. Lynden-Bell, in *Molecular Liquids, Dynamics and Interactions*, edited by A. J. Barnes, W. J. Orville-Thomas, and J. Yarwood (Reidel, Dordrecht, 1984).
[10] W. A. Steele, Adv. Chem. Phys. **34**, 1 (1976).
[11] J. Jang and R. M. Stratt, J. Chem. Phys. **112**, 7524 (2000), preceding paper.
[12] G. Goodyear and R. M. Stratt, J. Chem. Phys. **105**, 10050 (1996).
[13] M. Bruehl and J. T. Hynes, J. Phys. Chem. **96**, 4068 (1992).
[14] M. G. Kurnikova, D. H. Waldeck, and R. D. Coalson, J. Chem. Phys. **105**, 628 (1996).
[15] R. M. Stratt, Acc. Chem. Res. **28**, 201 (1995).
[16] T. Keyes, J. Phys. Chem. A **101**, 2921 (1997).
[17] R. E. Larsen, E. F. David, G. Goodyear, and R. M. Stratt, J. Chem. Phys. **107**, 524 (1997).
[18] B. M. Ladanyi and R. M. Stratt, J. Phys. Chem. **99**, 2502 (1995); **100**, 1266 (1996).
[19] B. M. Ladanyi and R. M. Stratt, J. Phys. Chem. A **102**, 1068 (1998).
[20] M. Buchner, B. M. Ladanyi, and R. M. Stratt, J. Chem. Phys. **97**, 8522 (1992).
[21] Integrating the average by parts, we have $I\overline{\Omega}^2=\langle\vec{N}(0)^2\rangle/2k_BT$, which is the exact friction at time zero. See, B. J. Berne and G. D. Harp, Adv. Chem. Phys. **17**, 63 (1970).
[22] G. Goodyear, R. E. Larsen, and R. M. Stratt, Phys. Rev. Lett. **76**, 243 (1996); G. Goodyear and R. M. Stratt, J. Chem. Phys. **107**, 3098 (1997).
[23] The most direct way to derive this equation is to note that, even in a molecular liquid, any translationally invariant probe function A will depend on just the intermolecular solvent-center-of-mass/solute-center-of-mass vectors $\vec{r}_{0j}=\vec{r}_j-\vec{r}_0$, and the various intramolecular vectors connecting the atomic sites with the molecular centers of mass. This dependence automatically implies that $\vec{\nabla}_0 A=-\Sigma_{j=1}^{N}\vec{\nabla}_j A$, where $\vec{\nabla}_k(k=0,...,N)$ refers to the gradients with respect to the solute-center-of-mass position $\vec{r}_0$ and the solvent-center-of-mass positions $\vec{r}_j$. Equation (2.14) then follows directly from the definition of the $c_{j\mu}$ coupling coefficients. Equivalently, we can think about the couplings in terms of the liquid's instantaneous

normal modes. Because our entire system is translationally invariant, there will always be three zero-frequency INM eigenvectors ($\gamma=x,y,z$) corresponding to net translation of the center of mass of the liquid as a whole in each of the three Cartesian directions. But, with any probe function A of the form described, the coupling c_γ to these translational modes will be identically zero. Substituting the components of these translational eigenvectors $U_{j\mu\gamma}$ into Eq. (2.13) and setting $c_\gamma=0$ also yields the relation (2.14). For a discussion of the role of translational invariance in INM spectra, see T.-M. Wu and R. F. Loring, J. Chem. Phys. **97**, 8568 (1992); Y. Wan and R. M. Stratt, *ibid.* **98**, 3224 (1993).

[24] $\mathbf{P}^b$ and $\mathbf{P}^{\perp b}$ satisfy the usual idempotent condition for projection operators ($\mathbf{PP}=\mathbf{P}$).

[25] The most strongly coupled solvent atom in a mode α is defined as the solvent atom j with the maximal value of the coupling strength C_j^α, where we define $C_j^\alpha=\Sigma_\mu(U_{j\mu,\alpha}-\sqrt{(m_j/M)}U_{0\mu,\alpha})c_{j\mu}$.

[26] B. J. Berne, M. E. Tuckerman, J. E. Straub, and A. L. R. Bug, J. Chem. Phys. **93**, 5084 (1990).

[27] M. Tuckerman and B. J. Berne, J. Chem. Phys. **98**, 7301 (1993).

[28] The excluded volume reported here is computed assuming a van der Waals radius of $\sigma/2$ for each atom in the diatomic.

[29] M. P. Allen and D. J. Tildesley, *Computer Simulation of Liquids* (Clarendon, Oxford, 1989).

[30] D. Fincham, Mol. Simul. **11**, 79 (1993).

[31] W. H. Press, S. A. Teukolsky, W. T. Vetterling, and B. P. Flannery, *Numerical Recipes in Fortran*, 2nd ed. (Cambridge University Press, Cambridge, 1992), Chap. 11.

[32] R. E. Larsen and R. M. Stratt, J. Chem. Phys. **110**, 1036 (1999).

[33] T. S. Kalbfleisch, L. D. Ziegler, and T. Keyes, J. Chem. Phys. **105**, 7034 (1996).

[34] R. Biswas, S. Bhattacharyya, and B. Bagchi, J. Chem. Phys. **108**, 4963 (1998).

[35] W. H. Press *et al.*, *Numerical Recipes in Fortran*, 2nd ed. (Cambridge University Press, Cambridge, 1992), Sec. 15.5.

[36] M. D. Stephens, J. G. Saven, and J. L. Skinner, J. Chem. Phys. **106**, 2129 (1997).

[37] We use solvent/solute-site distance as a criterion for determining the identity of the nearest neighbors. Because there are two separate atomic sites on our solute, we can therefore end up with either 1 or 2 nearest-neighbor solvent atoms.

[38] The fact that in Table IV we see two of the vibrational friction cases with components having greater than 100% weight arises from the presence of a small nonzero cross term in the particular projection used in this paper. The total coupling strength is a sum of the projected coupling, $C(\text{proj})$, its complement, $C(\text{comp})$, and a cross term, $C(\text{cross})$. However, within the projection scheme we are using for a solute with a finite mass, the cross term can in principle be negative, although the actual value is inevitably tiny. The end result is that it is possible to get $C(\text{proj})/C(\text{total})>1$.

[39] Defining the solute-site coordination number z as the integral $\rho\int d\vec{r}(r<r_{\min})g_{Av}(r)$ with ρ the solvent density, $g_{Av}(r)$ the solute-site/solvent radial distribution function, and $r_{\min}$ the location of the first minimum in $g_{Av}(r)$, we find $z=12.12$, 11.16, 14.56, 13.93, and 13.65 for bond lengths $d/\sigma=1.25$, 0.65, 0.325, 0.16, and 0.08, respectively.

[40] It is nonetheless perfectly possible for some spectroscopic manifestations of rotational and vibrational dynamics to appear to be independent of one another. See, A. Idrissi, M. Ricci, P. Bartolini, and R. Righini, J. Chem. Phys. **111**, 4148 (1999).

[41] A. Papazyan and M. Maroncelli, J. Chem. Phys. **102**, 2888 (1995).

[42] B. M. Ladanyi and R. M. Stratt, J. Chem. Phys. **111**, 2008 (1999).

[43] M. Bruehl and J. T. Hynes, Chem. Phys. **175**, 205 (1993).

[44] S. Gnanakaran and R. M. Hochstrasser, J. Chem. Phys. **105**, 3486 (1996); S. Gnanakaran, M. Lim, N. Pugliano, and R. M. Hochstrasser, J. Phys.: Condens. Matter **8**, 9201 (1996).

[45] R. G. Gordon, J. Chem. Phys. **44**, 1830 (1966).

[46] These jumps have also been interpreted as resulting from uncorrelated binary collisions taking place between the solvent molecules and the solute. See, D. Chandler, J. Chem. Phys. **60**, 3508 (1974).

[47] M. P. Allen and D. J. Tildesley, *Computer Simulation of Liquids* (Clarendon, Oxford, 1989), Sec. 3.3.2.